CHAPTER IV
RESULTS AND DISCUSSIONS

4.1 $27.5Gd_2O_3$-(72.5-x) B_2O_3-xDy_2O_3 glass system

The melt quenching technique was utilized to investigate the luminescence and physical properties of the gadolinium borate glasses that had been doped with Dy^{3+}.

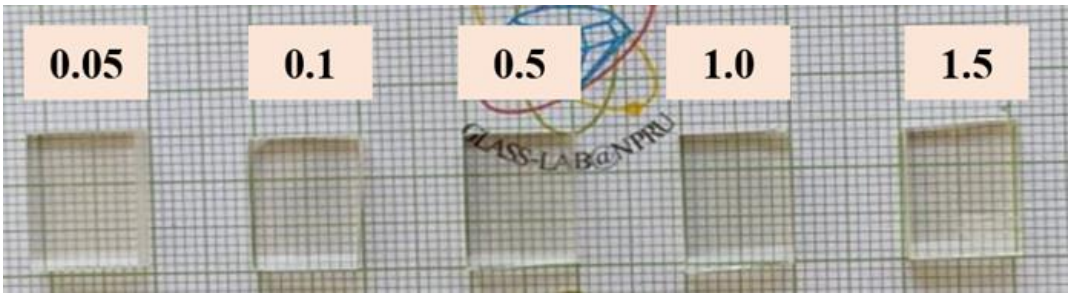

Figure 4.1 Image of glass samples containing $27.5Gd_2O_3$-(72.5-x) B_2O_3-xDy_2O_3 with various concentrations of Dy_2O_3.

The photos in Figure 4.1 are of samples of optically polished GBD glass. The glass sample gradually goes from clear to light yellow as Dy_2O_3 is added to it, as seen in the images (see Figure 4.1). Glass density is an essential characteristic to explore because of its wide range of variation in response to small changes in the glass structure. (Dias, J. D. M. et al., 2016; Kaewjaeng, S. et al., 2019).

4.1.1 Structural properties of lass

Figure 4.2 shows that no distinct peaks are present, which is evidence that the nature of these glasses is amorphous.

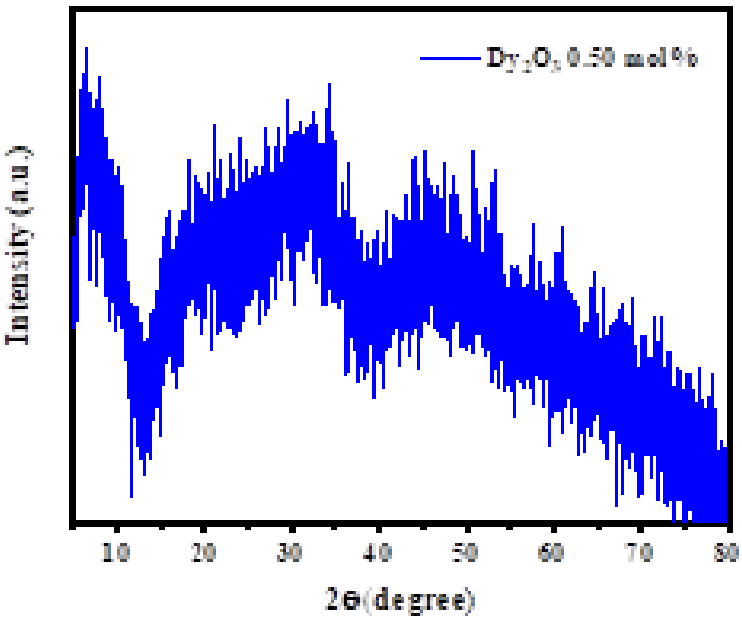

Figure 4.2 X-ray diffraction pattern of 0.5 mol% Dy_2O_3 content glass.

4.1.2 Physical properties

The primary source of knowledge regarding the structure and interactions of glass constituents is its physical properties. Therefore, precise measurement and exploration of these are required. All physical variables, including refractive indices (n), molar volume (V_M), and density (ρ).

The values for density and molar volume are displayed in Table 4.1. These numbers have a non-linear trend, as can be seen. Using Kaewjaeng et al., the polarizability of oxide ions was assessed. We noticed a non-linear trend in our glass's density and molar volume. This indicates that the addition of Dy_2O_3 content causes higher structural deterioration. Additionally, the molar volume is closely related to the oxygen distribution in the glass. (Umar, S. A. et al., 2017).

Table 4.1 The density and molar volume results of $27.5Gd_2O_3$-(72.5-x) B_2O_3-xDy_2O_3 glass system.

Sample	Density	Average Density	Molar volume	Average Molar volume
0.05	4.1180	4.1220 ± 0.0058	36.5017	36.4659 ± 0.0512
	4.1194		36.4889	
	4.1287		36.4072	
0.10	4.1632	4.1657 ± 0.0066	36.1414	36.1197 ± 0.0575
	4.1732		36.0546	
	4.1607		36.1631	
0.50	4.1943	4.1770 ± 0.0167	36.1631	36.3136 ± 0.1450
	4.1610		36.4525	
	4.1756		36.3252	
1.00	4.1328	4.1372 ± 0.0126	37.0685	37.0289 ± 0.1125
	4.1514		36.9019	
	4.1274		37.1162	
1.50	4.1940	4.1950 ±0.0140	36.8893	36.8808 ± 0.1226
	4.2094		36.7542	
	4.1815		36.9990	

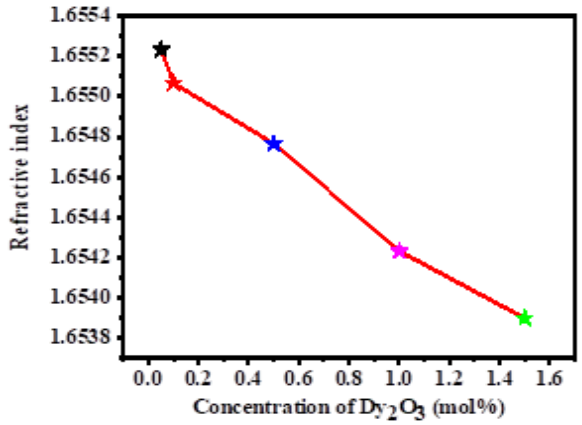

Figure 4.3 The refractive index relation of $27.5Gd_2O_3$-(72.5-x) B_2O_3-xDy_2O_3 glasses doped with varying concentrations of Dy_2O_3 ions.

As shown in Figure 4.3, the refractive index drops as the percentage of Dy_2O_3 increases. The increased density of the glasses is responsible for the observed drop in the glasses' refractive index. (Zaman, F. et al., 2019).

4.1.3 Fourier Transform Infrared Spectroscopy (FTIR)

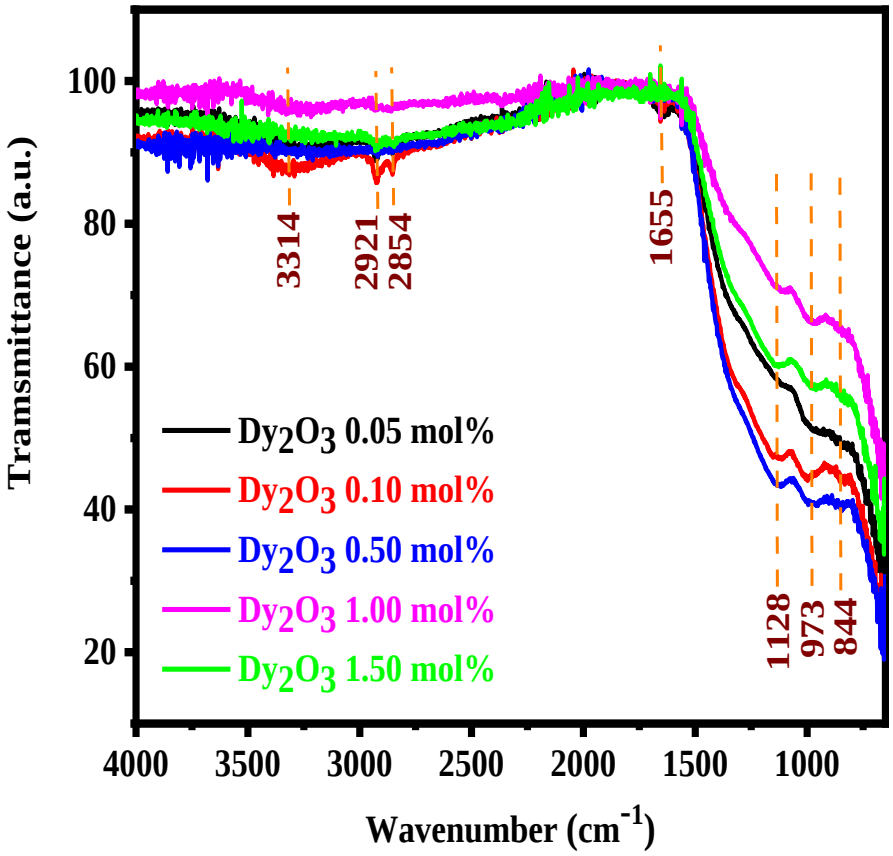

Figure 4.4 FTIR transmittance spectra of prepared glasses.

The FTIR band assignments of the obtained binary gadolinium borate glasses doped with Dy_2O_3 content may be seen in Figure 4.4 and Table 4.2. The range of these band assignments is from 600 to 4000 cm^{-1}.

Table 4.2 FTIR band spectral allocations of the glass system composed of $27.5Gd_2O_3$-(72.5-x) B_2O_3-xDy_2O_3.

Band position (cm^{-1})	Band Assignments
844	B–O bond stretching of tetrahedral BO_4 units (Balakrishna, A. et al., 2013)
973	B–O bond stretching of tetrahedral BO_4 units (Kaewjaeng, S. et al., 2021)
1128	B–O stretching vibrations of BO_4 units in tri-tetra and penta-borate groups (Lakshminarayana, G. et al., 2017)
1655	B–O bond stretching of trigonal BO_3units (Venugopal, A. R. et al., 2021)
2854 - 3314	H-O-H water groups (Ravangvong, S. et al., 2019)

4.1.4 UV-Vis-NIR Spectrophotometer

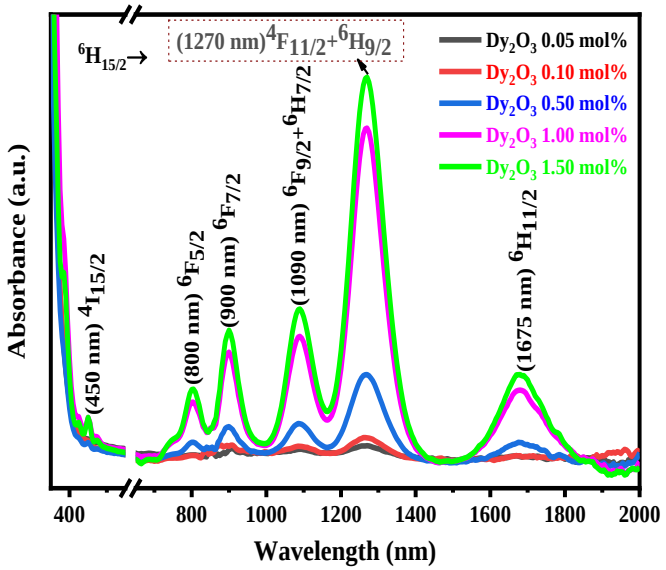

Figure 4.5 UV-Vis-NIR spectra of $27.5Gd_2O_3$-(72.5-x) B_2O_3-xDy_2O_3 glass system.

Because of the transition from the ground state of $^6H_{15/2}$ to several excited states, such as $^4I_{15/2}$, $^6F_{5/2}$, $^6F_{7/2}$, $^6F_{9/2}$+ $^6H_{7/2}$, $^6F_{11/2}$ + $^6H_{9/2}$ and $^6H_{11/2}$, respectively, the absorption spectra shown in Figure 4.5 exhibit dominant absorption peaks at 451, 800, 900, 1090, 1270, and 1675 nm. These peaks may be seen in the spectrum as 451, 800 (Luewarasirikul, N. et al., 2018)

4.1.5 Absorption Spectra

Figure 4.6 a. Samples made entirely of glass showed the characteristic Dy^{3+} signal. We recorded 11 Dy^{3+} ion peak crestings at 325, 350, 365, 387, 426, 452, and 472 nm and 4 Gd^{3+} ion peak crestings at 246, 253, 275, and 313 nm in the current glasses. Dy^{3+} and Gd3+ ions were found to have the most significant excitation peaks at 350 nm and 275 nm, respectively. The Dy^{3+} ion was directly excited at 350 and 275 nm, respectively, to examine the emission spectra. We see Gd^{3+} ion emission at 311 nm for 275 nm excitation; this emission is only detectable up to 0.5 mol% of Dy_2O_3, after which there is no further emission. Dy^{3+} ion emission was seen at 481, 576, 663, and 753 nm. Beyond 0.5 mol%, the emission intensity diminishes as more Dy_2O_3 content is added, with the highest emission intensity being reported for this content level. The concentration quenching effect is the cause of this decrease in intensity at high concentrations. (Rittisut W. et al., 2021)

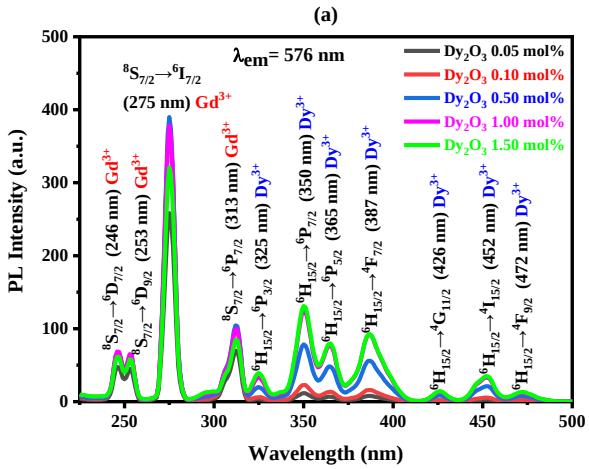

Figure 4.6 (a) Excitation spectra, (b) Emission spectra of $27.5Gd_2O_3$-(72.5-x) B_2O_3-xDy_2O_3 glass system monitored at 275 nm and (c) Emission spectra of $27.5Gd_2O_3$-(72.5-x) B_2O_3-xDy_2O_3 glass system monitored at 350 nm.

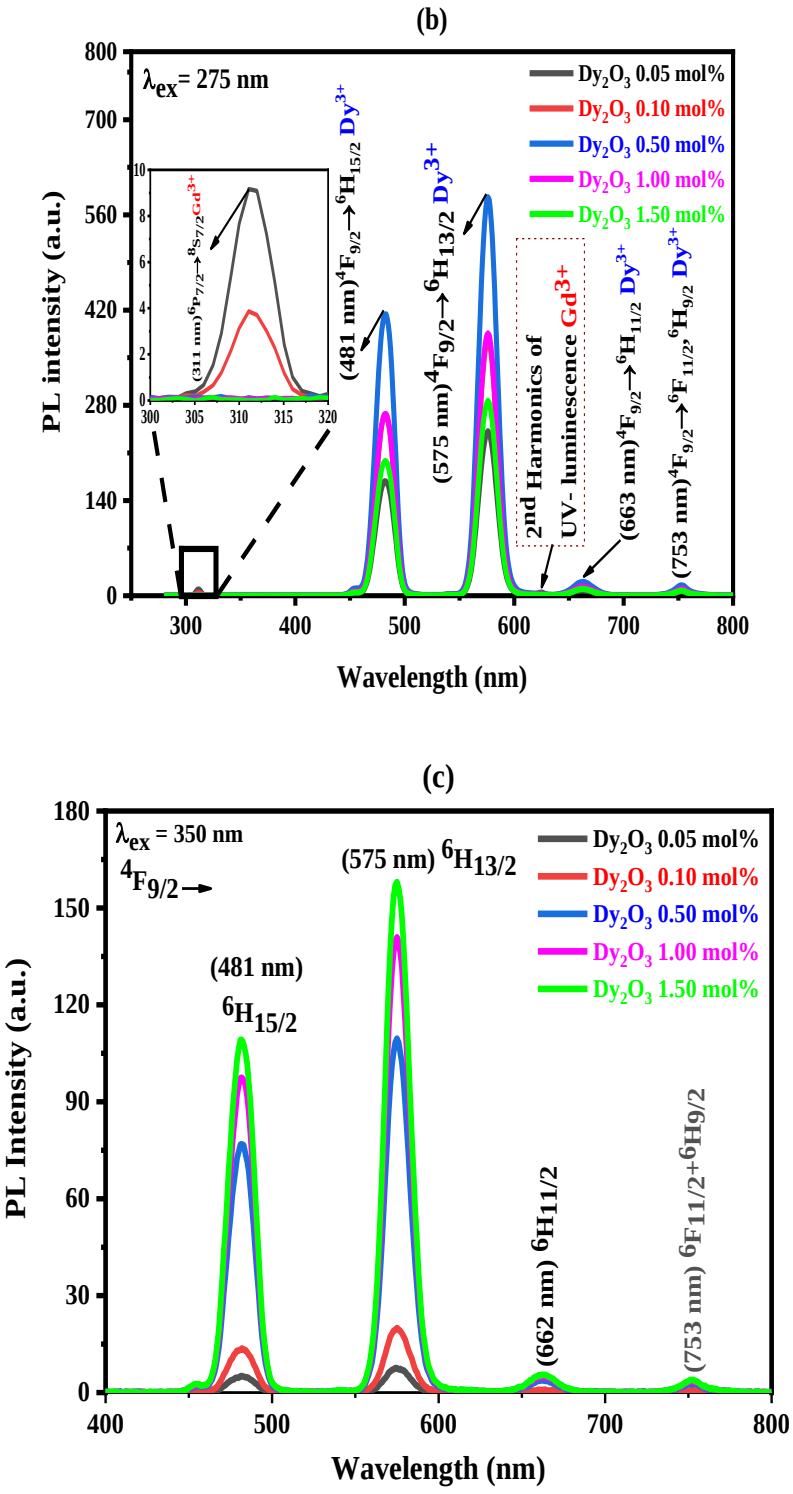

Figure 4.6 (Continued) (a) Excitation spectra, (b) Emission spectra of $27.5Gd_2O_3$-(72.5-x) B_2O_3-xDy_2O_3 glass system monitored at 275 nm and (c) Emission spectra of $27.5Gd_2O_3$-(72.5-x) B_2O_3-xDy_2O_3 glass system monitored at 350 nm.

4.1.6 Energy Transfer

When examined at 275 nm of Gd^{3+} ions, Figure 4.7(b) demonstrates that energy transfer (ET) can be observed from the $^6P_{7/2}$ transition of Gd^{3+} ions to the ^6F_J levels of Dy^{3+} ions. This was found to be the case. In addition, the $^6P_{7/2}$ to $^8S_{7/2}$ transition of Gd^{3+} ions was observed to produce fluorescence at the wavelength of 311 nm. At a concentration of 0.5 mol% Dy_2O_3, concentration quenching was not observed. This was because it prevented the opening of cross-relaxation channels (CRC) and resonance energy transfer (RET) in the non-radiative transition. This is shown in Figure 4.8.

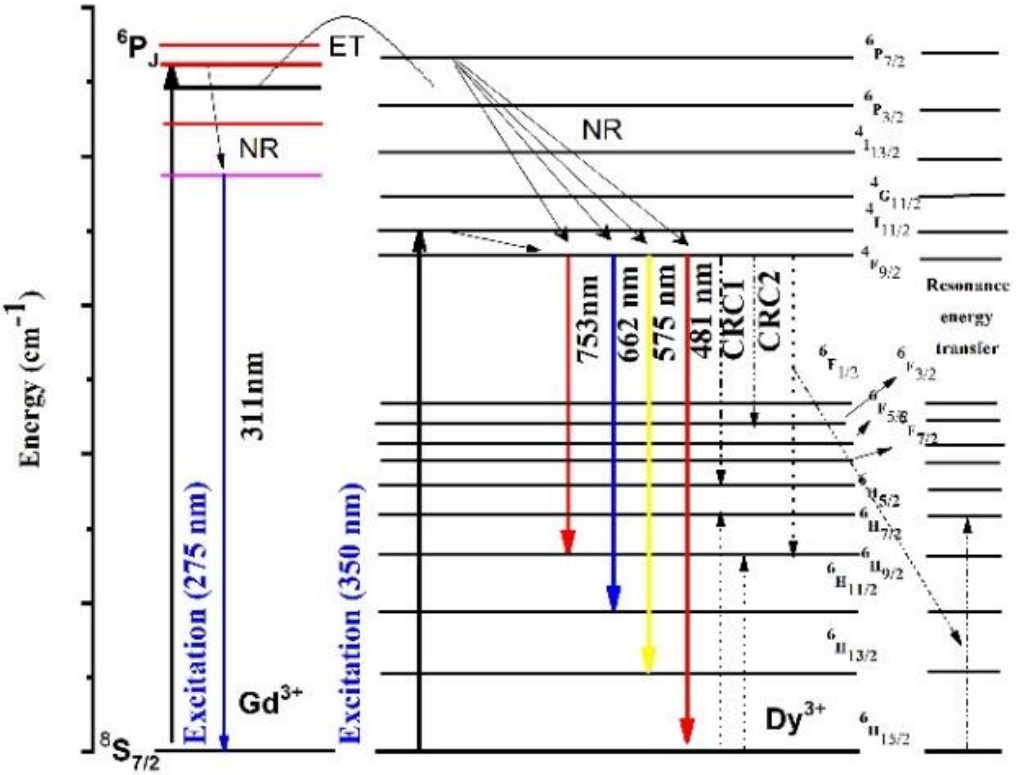

Figure 4.7 Diagrams depicting the transfer of energy from Gd^{3+} ions to Dy^{3+} ions.

4.1.7 Photoluminescence excitation and emission (PLEs) spectra

Figures 4.9(a) and 4.9(b) illustrate the emission intensity (576 nm) of Dy_2O_3 concentration at 275 nm and 350 nm excitations, respectively.

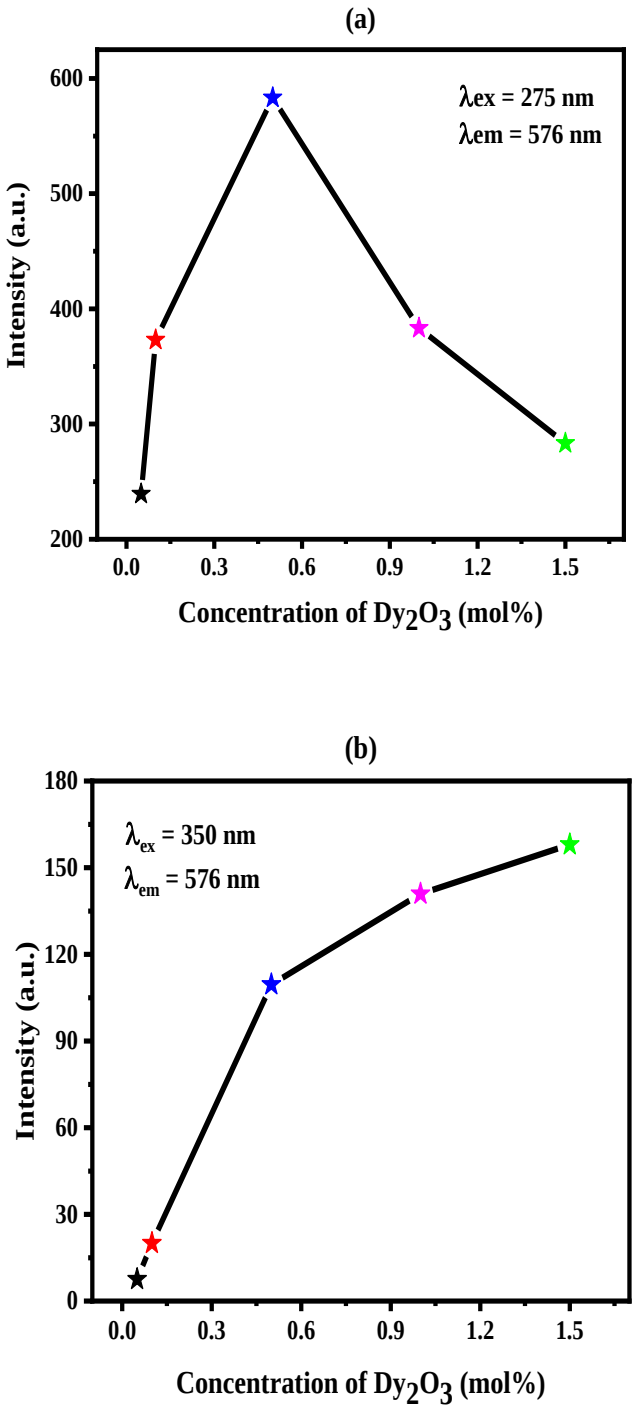

Figure 4.8 (a) The relationship between the emission intensity at 576 nm and the content of Dy_2O_3 in the prepared glass samples when excited at 275 nm and (b) The relationship between the concentration of Dy_2O_3 in the produced glass samples and the emission intensity at 576 nm.

4.1.8 Decay Time

The decay time profile depicted in Figure 4.10 exhibits single exponential behavior. The increased resonance energy transfer through cross-relaxation and resonant energy transfer was responsible for the observed drop in decay durations from 0.680 to 0.492 ms with increased Dy_2O_3 content. (Zaman, F. et al., 2019).

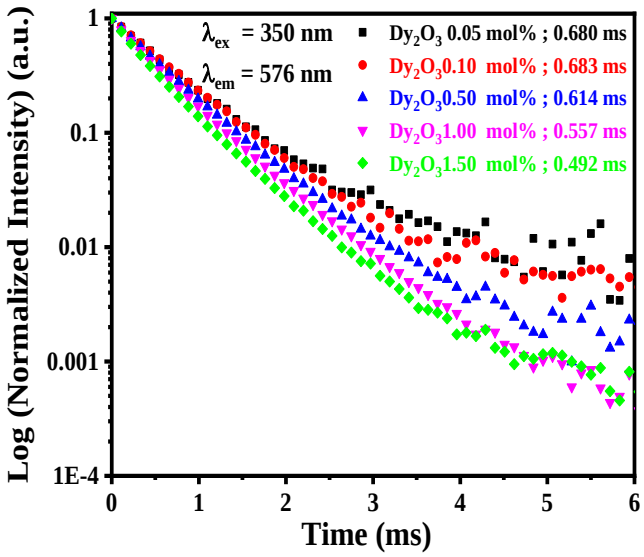

Figure 4.9 The Decay time profile of $27.5Gd_2O_3$-(72.5-x) B_2O_3-xDy_2O_3 glass system.

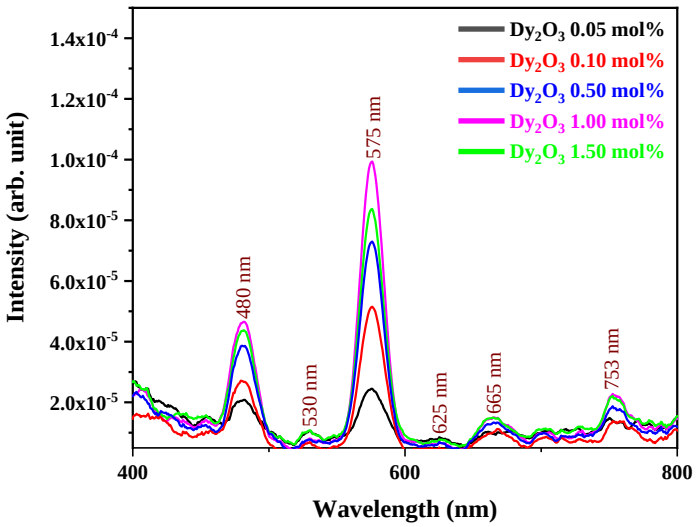

Figure 4.10 Radioluminescence of Dy_2O_3 concentrations in $27.5Gd_2O_3$-(72.5-x)B_2O_3-xDy_2O_3 (GBD) glasses.

4.1.9 CIE chromaticity coordinates and color correlated temperature (CCT)

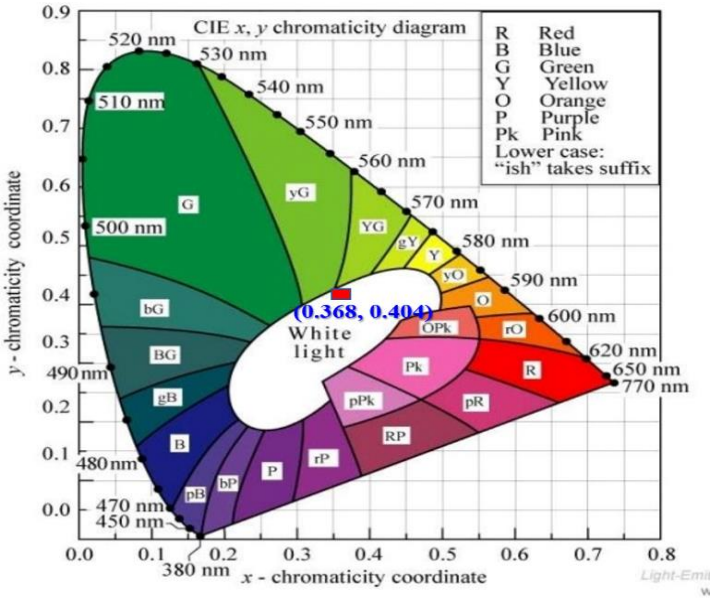

Figure 4.11 CIE coordinate diagram of $27.5Gd_2O_3$-(72.5-x) B_2O_3-xDy_2O_3 glasses doped with varying concentrations of Dy_2O_3.

Figure 4.12 illustrates the results, which show that the x and y color coordinates of the emission spectra of glasses doped with Dy_2O_3 may be obtained from a precise location of about (0.368 and 0.404). The data illustrate this.

4.1.10 Application of Blue LED Encapsulation

The CIE diagram demonstrated that the made glass sample emits white light with an excitation of 350 nm. This finding hint that the model may find application in white light emitting devices (WLEDs), also known as white light emitting diodes. Figure 4.13 is a diagram that illustrates the encapsulation of the studied glass into a UV (blue) LED. This diagram is in the form of a schematic. As can be seen, the color of light emitted by the glass is white, as shown in Figures 4.13(a)–4.13(c).

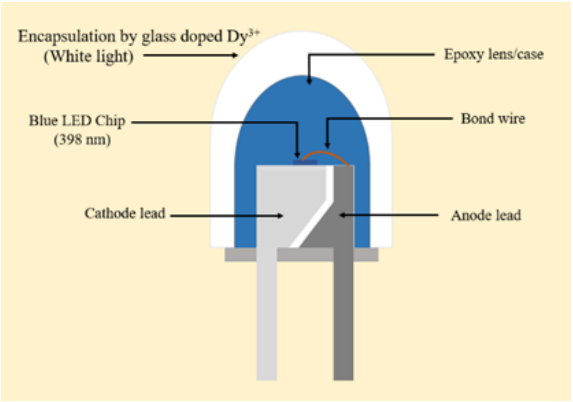

Figure 4.12 Schematic diagrams showing the Encapsulation of prepared glass on Blue LED.

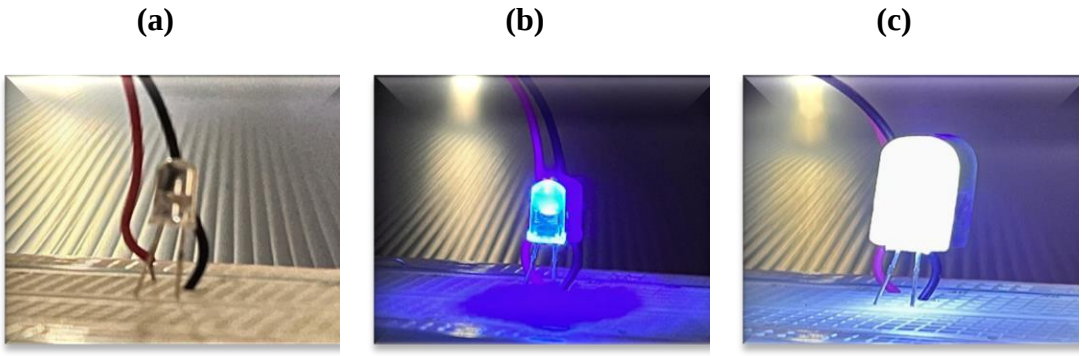

Figure 4.13 Encapsulation of studied glass with Blue LED. (a) Before encapsulation of glass with Blue LED, (b) Blue LED powered with 3.0 volts and (c) Glass encapsulated on Blue LED powered with 3.0 volts.

As can be seen in Figures 4.13 and 4.14, the bell-shaped glasses have been constructed by our team to encase a blue LED within them. As shown in Figure 4.14(a), the circuitry for the system was fabricated by connecting a breadboard rated for 3.0 volts to a blue LED. As shown in Figure 4.14(b), the connection was given an "on" switch to light the blue LED (398 nm). The encapsulation of a prepared bell-shaped glass sample is shown in Figure 4.14(c) on top of a blue LED. When the connection was turned "on," the LED lit up with a warm white light, suggesting that these glasses could be employed as encapsulating materials. (Shasmal, N. et al., 2019; Rajaramakrishna, R. et al., 2020; Boonpa, W. et al., 2022).